AC conductivity for a holographic Weyl semimetal

Gianluca Grignani, Andrea Marini, Francisco Peña-Benitez and Stefano Speziali

Dipartimento di Fisica e Geologia, Università di Perugia,
I.N.F.N. Sezione di Perugia,
Via Pascoli, I-06123 Perugia, Italy

E-mail: gianluca.grignani@pg.infn.it, andrea.marini@pg.infn.it, benitez@pg.infn.it, stefano_speziali@libero.it

Abstract: We study the AC electrical conductivity at zero temperature in a holographic model for a Weyl semimetal. At small frequencies we observe a linear dependence in the frequency. The model shows a quantum phase transition between a topological semimetal (Weyl semimetal phase) with a non vanishing anomalous Hall conductivity and a trivial semimetal. The AC conductivity has an intermediate scaling due to the presence of a quantum critical region in the phase diagram of the system. The phase diagram is reconstructed using the scaling properties of the conductivity. We compare with the experimental data of [1] obtaining qualitative agreement.

Contents

1 Introduction

The recent discovery of Weyl semimetals (WSM) [2] has increased the interest of both high energy and condensed matter communities in their description. WSM are three dimensional gapless semiconductors. Their low energy excitations are massless fermions, called Weyl fermions. Due to the Nielsen-Ninomiya theorem [3] these fermions come in pairs with opposite chirality (right- and left-handed). In some sense these materials can be viewed as a 3d version of graphene. WSM are characterized by the presence of singular points in the Brillouin zone where the conduction and valence band touch. If time reversal or parity is broken, left- and right-handed quasiparticles can sit at different points in the Brillouin zone. The fact that quasi-particles around the Weyl points obey a massless relativistic equation implies astonishing properties for these materials, as chiral magnetic [4–6] and vortical effects [7–10], odd (Hall) viscosity [11], negative magnetoresistivity [12–14]. All these phenomena are intimately related with the quantum anomalies observed in massless fermionic systems. Another characteristic property of WSM is the presence of edge states, called Fermi arcs [2, 15].

As it happens in graphene, the Fermi velocity of the electrons in WSM is at least two orders of magnitude smaller than the speed of light [16]. Therefore the analogue of the

fine structure constant can be a hundred times bigger than its QED counterpart, opening the possibility of the strong coupling regime. However, most of the attempts to describe WSM have been from a weakly coupled perspective [17–20]. From a strong coupling point of view some effort has also been done [16, 21–24].

At zero temperature Weyl materials are supposed to show quantum phase transitions connecting quantum anomalous Hall insulators, insulators and the Weyl semimetal phases [17].

Inspired by the recent experiment[1] [1], we studied the optical response of a strongly coupled Weyl semimetal using holography. From a holographic point of view, the problem of the optical conductivity has been already addressed in the past [22], however the aspects of having a splitting of Weyl cones was ignored, also the presence of the chiral anomaly was not implemented. For these reasons, we choose the perspective of [23], in which separation of the Weyl cones and the axial anomaly are effectively implemented.

The observations of [1] are partially consistent with the weak coupling predictions of [17, 19]. For frequencies higher than the temperature of the material, the conductivity is characterized by a straight line that changes its slope at some energy scale. The first slope is consistent with the prediction [19]

$$\sigma \approx n \frac{e^2}{12h} \frac{\omega}{v_f}, \tag{1.1}$$

in which $n = 8$ is the number of Weyl points around the Fermi energy. They used this expression to fit the value of the Fermi velocity, obtaining a value consistent with previous predictions for this material. The second slope is interpreted as a changing in number of degrees of freedom due to the presumable influence of the rest of Weyl points at such energies. Nonetheless in this case the Fermi velocity obtained does not lie within a reasonable value. Certainly there could be many effects influencing the intermediate behavior of the conductivity, however the robust persistence of a power law at those energies suggests that the physics of the Weyl cones is still determining the optical response. An alternative explanation implied by our toy model could be given by the presence of the quantum critical point and its corresponding quantum critical region.

The rest of the paper is organized as follows. In section 2 we review and generalize the model of [23]. Then, in section 3, we classify the IR geometries, which are dual to the ground states of the system. In section 4 we compute analytically the IR frequency dependence of the conductivity for the different phases of the model, and numerically the full frequency dependence of the conductivity matrix. We also reconstruct the quantum phase diagram of the model using the power law properties of the conductivity. In section 5 we compare our results with [1] and we finish with our conclusions.

Note added. When finishing the paper we received the manuscript [25] which shows some overlap with our work. They studied the anomalous Hall conductivity in the axial current and considered a top down model.

---

[1]We acknowledge Maria A. H. Vozmediano for letting us know about the existence of this paper.

2 Holographic effective theories for a Weyl semimetal

A holographic model for Weyl semimetals has been proposed in [23] and studied in more detail in [24] and [11]. The main features of this model are the implementation of the chiral anomaly and effective separation of Weyl cones. The model undergoes a quantum phase transition from a topologically non-trivial semimetal to a trivial one. Previous holographic models [21, 22, 26] have considered a semi-holographic point of view, coupling weakly coupled Weyl fermions to a strongly coupled quantum critical system.

We shall follow the spirit of [23] to implement a time-reversal breaking parameter[2] and a "mass operator", as deformations of a strongly coupled conformal field theory. The holographic action we propose is a generalization of the action used in [23]

$$S = S_0 + S_{GH} + S_{CT} \tag{2.1}$$

$$S_0 = \int d^5x \sqrt{-g} \left[R - \mathcal{V}(|\phi|) - \frac{1}{4}Z_1(|\phi|)H^2 - \frac{1}{4}Z_2(|\phi|)F^2 - Z_3(|\phi|)|D\phi|^2 \right.$$
$$\left. + \frac{\alpha}{3}\epsilon^{MNRPQ}A_M(F_{NR}F_{PQ} + 3H_{NR}H_{PQ}) \right], \tag{2.2}$$

where $\epsilon_{MNRPQ} = \sqrt{-g}\varepsilon_{MNRPQ}$ and $\varepsilon_{0123r} = 1$. S_{GH} and S_{CT} are the Gibbons-Hakwing boundary action and the counterterm that renormalizes the on-shell action, respectively. We show them in appendix A.

In Holography, currents associated to global symmetries of the QFT are dual to gauge fields propagating in the five dimensional geometry, whereas quantum anomalies are implemented by Chern Simons terms in the action [27]. Let us explain the ingredients of the model:

- The field dual to the vector (electromagnetic) boundary current is V_M and $H_{MN} = \partial_M V_N - \partial_N V_M$ its corresponding field strength. The asymptotic value of V_M is the source for the electromagnetic current, i.e. it corresponds to a non dynamical background electromagnetic field switched on in the dual field theory.

- A_M is the field dual to the (anomalous) axial current and its corresponding field strength is $F_{MN} = \partial_M A_N - \partial_N A_M$. The boundary value of A_M is the source for the anomalous axial current.

- The Chern Simons coupling has been properly tuned in order to reproduce the Ward's identities of the *consistent* (conserved) vector and (anomalous) axial currents of the boundary QFT [23]

$$\partial_\mu J^\mu = 0, \tag{2.3}$$

$$\partial_\mu J_5^\mu = -\frac{\alpha}{3}\varepsilon^{\mu\nu\rho\lambda}(F_{\mu\nu}F_{\rho\lambda} + 3H_{\mu\nu}H_{\rho\lambda})\ldots \tag{2.4}$$

where dots refer to the contribution coming from the explicit breaking of $U(1)_{axial}$ given by the presence of the mass deformation. Comparing the Ward identity for N

---

[2]Effective separation of Weyl cones.

Dirac fermions with eq. (2.4) we can fix the Chern-Simons coupling to be

$$\alpha = \frac{N}{16\pi^2},\tag{2.5}$$

N is the flavor number.

- In order to have a conformal UV fixed point, i.e. an asymptotically AdS space the scalar potential has to satisfy

$$\mathcal{V}_{\text{UV}} \equiv \mathcal{V}(|\phi_{\text{UV}}|) = -\frac{12}{L^2}\,.\tag{2.6}$$

- The holographic dictionary establishes that the scalar field ϕ is dual to a certain scalar operator $\mathcal{O}$ with scaling dimension $[\mathcal{O}] = \Delta_\phi$ given by

$$\Delta_\phi = 2 + \sqrt{4 + (mL)^2}\,,\tag{2.7}$$

where $m^2 = 1/2\mathcal{V}''_{\text{UV}}$. If we choose $(mL)^2 = -3$,[3] the operator $\mathcal{O}$ will have scaling dimension $\Delta_\phi = 3$ and necessarily will couple to a source M of dimension $[M] = 1$. So we are allowed to interpret the scalar field as a mass deformation of the CFT.

- The scalar field is charged only under the axial field, and the covariant derivative reads $D_M = \partial_M - iqA_M$. Notice that if the scalar field were charged under the vector field V_M the electromagnetic current would not be conserved.

Writing the scalar field as $\phi = \psi e^{i\theta}$, the gauge invariance of the system allows us to set $\theta = 0$. In this way the action can be written as follows

$$S_0 = \int \mathrm{d}^5 x \sqrt{-g} \bigg[R - \mathcal{V}(\chi) - \frac{1}{4}Z_1(\chi)H^2 - \frac{1}{4}Z_2(\chi)F^2 - (\partial\chi)^2 + W(\chi)A^2$$
$$+ \frac{\alpha}{3}\epsilon^{MNRPQ}A_M\big(F_{NR}F_{PQ} + 3H_{NR}H_{PQ}\big)\bigg]\,,\tag{2.8}$$

where the new scalar field is defined by $\partial_\chi \psi(\chi) = (Z_3(\chi))^{-1/2}$ and $W(\chi) = q^2\psi^2 Z_3$.

Considering that we already proved that (2.1) is contained in (2.8), we will use (2.8) as the fundamental action without assuming any specific form for the functions $\mathcal{V}, Z_1, Z_2, W$. The holographic dictionary establishes that the on-shell gravity action corresponds to the generating functional of the QFT. Therefore, taking variations of the action with respect to the sources we obtain the one-point functions of the corresponding associated operators

$$J^\mu = \frac{\delta S}{\delta v_\mu}\,, \qquad J_5^\mu = \frac{\delta S}{\delta b_\mu}\,, \qquad \mathcal{O} = \frac{\delta S}{\delta M}\,,\tag{2.9}$$

where $v_\mu = V_\mu(\Lambda)$, $b_\mu = \Lambda^{-\Delta_b}A_\mu(\Lambda)$,[4] and $M = \Lambda^{4-\Delta_\phi}\chi(\Lambda)$ are the field theory sources. Λ is the UV radial cutoff where we put the field theory to live before renormalising and sending it to infinity.

---

[3]Notice that AdS BF bound $(mL)^2 > -4$ is not violated for this mass.

[4]The scaling dimension of J_5 is $[J_5] = 3 + \Delta_b$, with $\Delta_b = -1 + \sqrt{1 + \frac{2W_{\text{UV}}L^2}{Z_2(UV)}}$. Notice that in the case of the abelian Higgs action (2.1) $\Delta_b = 0$. For simplicity, and assuring that the explicit U(1)$_{\text{axial}}$ breaking is only due to the presence of the scalar mass operator we will assume $W(\chi_{\text{UV}}) = 0$. We will also assume $Z_1(\chi_{\text{UV}}) = Z_2(\chi_{\text{UV}}) = 1$.

Taking variations of the renormalized action (2.8), we obtain the consistent currents and scalar operator

$$J^\mu = \lim_{\Lambda \to \infty} \left[\sqrt{-g} Z_1 H^{\mu r} + 4\alpha \varepsilon^{\mu\nu\rho\lambda} A_\nu H_{\rho\lambda} \right]_\Lambda + \frac{\delta S_{CT}}{\delta v_\mu} \,, \tag{2.10}$$

$$J_5^\mu = \lim_{\Lambda \to \infty} \left[\sqrt{-g} Z_2 F^{\mu r} + \frac{4}{3}\alpha \varepsilon^{\mu\nu\rho\lambda} A_\nu F_{\rho\lambda} \right]_\Lambda + \frac{\delta S_{CT}}{\delta b_\mu} \,, \tag{2.11}$$

$$\mathcal{O} = -2 \lim_{\Lambda \to \infty} \Lambda^{\Delta_\phi - 4} \sqrt{-\gamma} \, \partial_r \chi \Big|_\Lambda + \frac{\delta S_{CT}}{\delta M} \,. \tag{2.12}$$

3 IR fixed points

As it is well known, this type of theories may have an RG flow from the UV AdS fixed point to other scaling fixed points in the IR, where the flow is tuned by the running of the scalar field [28–32]. In our analysis we will consider the case where the scalar runs to a constant. On top of that, the authors of [24] proved that the IR behavior of the solution determines whether the system is in a Weyl semimetal or in a trivial semimetal phase, depending on whether the spatial component of the axial gauge field runs to a constant or to zero. Restricting to the case of neutral zero temperature IR geometries we propose the following ansatz

$$ds^2 = u(r)(-dt^2 + dx_1^2 + dx_2^2) + h(r)dx_3^2 + \frac{dr^2}{u(r)} \,, \tag{3.1}$$

$$A = A_3(r)dx_3 \,, \tag{3.2}$$

$$\chi = \chi(r) \,, \tag{3.3}$$

The equations of motion of the system are shown in the appendix B. As previously pointed out, we look for scaling IR geometries with constant scalar field at the leading order, $\chi(r) = \chi_{\text{IR}} + \delta\chi(r)$. Therefore we assume the following form for the IR metric components[5]

$$u(r) = u_0 r^2 \left(1 + \delta u(r)\right) \,, \qquad h(r) = h_0 r^{2\beta} \left(1 + \delta h(r)\right) \,, \tag{3.4}$$

together with the consistency conditions[6]

$$u_0 > 0 \,, \qquad h_0 > 0 \,, \qquad Z_2^{\text{IR}} > 0 \,. \tag{3.5}$$

With these assumptions, the leading order IR Einstein's equations take the form

$$\frac{W_{\text{IR}}}{2h_0 u_0} \left(\frac{A_3}{r^\beta}\right)^2 - \frac{Z_2^{\text{IR}}}{4h_0} \left(\frac{A_3'}{r^{\beta-1}}\right)^2 + \frac{\mathcal{V}_{\text{IR}}}{2u_0} + 3(\beta+1) = 0 \,, \tag{3.6}$$

$$\frac{Z_2^{\text{IR}}}{2h_0} \left(\frac{A_3'}{r^{\beta-1}}\right)^2 - (1-\beta)\beta = 0 \,, \tag{3.7}$$

$$\frac{Z_2^{\text{IR}}}{2h_0} \left(\frac{A_3'}{r^{\beta-1}}\right)^2 - \frac{W_{\text{IR}}}{h_0 u_0} \left(\frac{A_3}{r^\beta}\right)^2 - (1-\beta)(\beta+3) = 0 \,. \tag{3.8}$$

These equations can be consistently solved for two possible cases:

---

[5]Using this radial coordinate the IR region is located at $r \to 0$.

[6]Notice that we have included subleading corrections to the IR fields; knowing the form of the corrections is necessary to understand the reliability of the IR solution.

- *Critical or Marginal solution:* if $A_3(r) = r^\beta (1 + \delta A_3(r))$ the equations become an algebraic system that can be solved exactly for u_0 and h_0

$$u_0 = -\frac{\mathcal{V}_{\mathrm{IR}}}{9 + \beta(\beta + 2)}, \quad h_0 = \frac{\beta}{2(1 - \beta)} Z_2^{\mathrm{IR}}. \tag{3.9}$$

The Maxwell and scalar equations reduce to

$$W_{\mathrm{IR}} = \frac{3}{2} \beta Z_2^{\mathrm{IR}} u_0, \quad \partial_\chi \log\left(\mathcal{V} W^{3p} Z^{\beta p}\right)|_{\chi = \chi_{\mathrm{IR}}} = 0, \tag{3.10}$$

with $p = \frac{\beta - 1}{\beta^2 + 2\beta + 9}$, which can be used to solve for β and χ_{IR}. The consistency conditions imply

$$\mathcal{V}_{\mathrm{IR}} < 0, \qquad 0 < \beta < 1. \tag{3.11}$$

See appendix C for an analysis of perturbations around the IR geometries.

- *Irrelevant solutions:* the second possibility corresponds to the gauge field decaying in the IR fast enough such that $r^{-\beta} A_3$ is subleading in the IR. They can be split in two disconnected cases, depending on whether the gauge field vanishes or not in the IR.

  - *Trivial semimetal:* if the gauge field vanishes, the solution for eqs. (3.6)–(3.8) is AdS, with the IR length scale given by

  $$u_0 = -\frac{1}{12} \mathcal{V}_{\mathrm{IR}} = L_{\mathrm{IR}}^{-2}, \qquad \beta = 1. \tag{3.12}$$

  Then, using the scalar equation, the value for χ_{IR} is fixed by minimizing $\mathcal{V}$ and the Maxwell equation trivializes

  $$\mathcal{V}'(\chi_{\mathrm{IR}}) = 0, \qquad \mathcal{V}_{\mathrm{IR}} < 0. \tag{3.13}$$

  If we consider the leading corrections to AdS that preserve $T = 0$ and are irrelevant in the IR, we obtain

  $$\delta A_3 = c_b r^{\Delta_{b_{\mathrm{IR}}}}, \qquad \delta \chi = c_\chi r^{-4 + \Delta_{\chi_{\mathrm{IR}}}}, \tag{3.14}$$

  with the IR scaling dimension of the associated operators

  $$\Delta_{b_{\mathrm{IR}}} = -1 + \sqrt{1 + \frac{2 W_{\mathrm{IR}} L_{\mathrm{IR}}^2}{Z_2^{\mathrm{IR}}}}, \qquad \Delta_{\chi_{\mathrm{IR}}} = 2 + \sqrt{4 + m_{\mathrm{IR}}^2 L_{\mathrm{IR}}^2}. \tag{3.15}$$

  Stability of the IR background requires

  $$W_{\mathrm{IR}} > 0, \qquad m_{\mathrm{IR}}^2 L_{\mathrm{IR}}^2 > 0. \tag{3.16}$$

  - *Weyl semimetal phase:* there is a last inequivalent irrelevant case. If the gauge field runs to a constant, necessarily eqs. (3.6)–(3.8) imply that the gauge field must be massless in the IR

  $$W_{\mathrm{IR}} = 0. \tag{3.17}$$

If the last is satisfied, the solution is AdS

$$u_0 = -\frac{1}{12}\mathcal{V}_{\text{IR}}, \qquad \beta = 1, \qquad \mathcal{V}_{\text{IR}} < 0, \tag{3.18}$$

the peculiarity of this solution is that the scalar field must be simultaneously an extremum of the scalar potential and the mass function

$$\mathcal{V}'(\chi_{\text{IR}}) = 0, \qquad W'(\chi_{\text{IR}}) = 0, \tag{3.19}$$

Perturbations show an irrelevant deformation,

$$\delta\chi = c_\chi r^{-3/2} e^{-\frac{s}{r}}, \tag{3.20}$$

with $s = \sqrt{1/2 W''_{\text{IR}} h_0^{-1}} L_{\text{IR}}$ and $W''_{\text{IR}} > 0$. If the last inequality was not satisfied, the Weyl semimetal phase would not be reliable considering that all perturbations would be relevant.

The previous analysis allowed us to have a geometrical picture of the Weyl semimetal phase. Let us remind the reader that gauge symmetries in the bulk correspond to global symmetries in the boundary theory, therefore the condition $W_{\text{IR}} = 0$ means that axial gauge symmetry is restored in the IR. On the other hand, the trivial phase is characterized by a massive axial gauge field in the IR, such that gauge symmetry is explicitly broken, giving an IR anomalous dimension to the operator J_5 determined by (3.15). That explains why the minimal coupling of the abelian Higgs model used by [24] contains the Weyl semimetal phase.

4 Conductivities

Before computing the full frequency dependence of the conductivity, for which it will be necessary to use numerical techniques, we will analyze the behavior at small frequencies. To do so, we introduce the following consistent set of linear fluctuations

$$\delta V_i = v_i(r)\, e^{-i\omega t} \tag{4.1}$$

where i takes values x, y, z. The fluctuations are decomposed into two sectors, longitudinal and transverse to the background $A_M = (0, 0, 0, A_3, 0)$. The transverse equations read

$$\left(u\sqrt{h}Z_1 v'_c\right)' + \left(\omega^2 \frac{Z_1\sqrt{h}}{u}\delta_{cd} + 8i\omega\alpha A'_3\epsilon_{cd}\right) v_d = 0, \tag{4.2}$$

with $c, d = x, y$. These equations can be diagonalized using the helicity fields $v_\pm = v_x \pm i v_y$

$$\left(u\sqrt{h}Z_1 v'_\pm\right)' + \left(\omega^2 \frac{Z_1\sqrt{h}}{u} \pm 8\omega\alpha A'_z\right) v_\pm = 0. \tag{4.3}$$

The equation for the longitudinal field can be written as

$$\left(\frac{u^2}{\sqrt{h}}Z_1 v'_z\right)' + \frac{\omega^2 Z_1}{\sqrt{h}} v_z = 0. \tag{4.4}$$

These equations were studied in [24] to compute the DC conductivities in the case $Z_1 = Z_2 = 1$ and $W = q^2\chi$. In this section we shall generalize their computation and we will also obtain the leading ω behavior of the conductivities.

4.1 DC conductivities

We start first by computing the DC conductivities solving eqs. (4.3), (4.4) up to linear order in ω. To do so, we construct a perturbative solution as follows

$$v(r) \approx v^{(0)}(r) + \omega \, v^{(1)}(r) + O(\omega)^2 \,. \tag{4.5}$$

The solution for $v^{(0)}(r)$ and $v^{(1)}(r)$ can be found in an integral form even though the explicit functions of the background fields are not know analytically. After imposing regularity of fields in the IR, we obtain the linear order solutions

$$v_z(r) \approx 1 + \mathcal{O}(\omega)^2 \tag{4.6}$$

$$v_\pm(r) \approx 1 \mp 8\alpha\omega \int_r^\infty \mathrm{d}r' \frac{A_3(r') - A_3(0)}{u(r')\sqrt{h(r')}Z_1(\chi(r'))} + O(\omega)^2 \,. \tag{4.7}$$

Using the definition (2.10) we can write the *consistent* current as follows

$$J_i = \lim_{\Lambda \to \infty} \left(-\Lambda^3 \frac{i}{\omega} \frac{v_i'(\Lambda)}{v_k(\Lambda)} + 8\alpha\epsilon_{ijk}b_j - i\omega\delta_{ik}\log\Lambda \right) (i\omega v_k(\Lambda)) \,, \tag{4.8}$$

from which we read the conductivity. After plugging the solutions (4.6), (4.7) into (4.8) and using $u = h = r^2$, $\chi = 0$, the only non vanishing conductivity is the anomalous Hall

$$\sigma_{AH} = 8\alpha A_3(0) = 8\alpha b_{\mathrm{IR}} \,. \tag{4.9}$$

It is important to emphasize that, as it generally happens with anomaly induced transport coefficients, the form of (4.9) is not modified by considering general $\mathcal{V}, Z_1, Z_2, W$, showing the universality of the anomalous Hall conductivity. It is only necessary a non vanishing value of the axial field in the IR to have a non vanishing anomalous Hall conductivity, as expected. The other conductivities vanish, nonetheless we are interested in estimating their small ω dependence. In order to do so, it is necessary to change strategy and use the matching asymptotic technique.

4.2 IR scaling of longitudinal and transverse conductivities

If we plug the ansatz (3.4) into the eq. (4.4), change coordinates and redefine fields as follow

$$r = \frac{\omega}{u_0 x} \,, \qquad v_z = x^{\frac{3-\beta}{2}} p \tag{4.10}$$

the e.o.m. acquires the form of a Bessel equation

$$x^2 p''(x) + x p'(x) + \left(x^2 - \nu_1^2 \right) p(x) = 0 \,, \tag{4.11}$$

with $\nu_1 = \frac{3-\beta}{2}$. The solution satisfying the infalling condition is the Hankel function

$$p(x) = H_{\nu_1}(x) \,. \tag{4.12}$$

With this solution and following [28, 33, 34] the small frequency behavior can be obtained

$$\mathrm{Re}\,\sigma_{zz} \propto \omega^{2|\nu_1|-1} = \omega^{2-\beta} \,. \tag{4.13}$$

To solve eq. (4.3) we notice that for the irrelevant solutions the Chern-Simons contribution in the equation is subleading whereas in the critical case it is not. Again changing variables

$$v_\pm = x^{\frac{1+\beta}{2}} q_\pm \,, \tag{4.14}$$

the equations read

$$x^2 q''_\pm(x) + x q'_\pm(x) + \left(x^2 - 1\right) q_\pm(x) = 0 \,, \qquad \beta = 1 \tag{4.15}$$

$$x^2 q''_\pm(x) + x q'_\pm(x) + \left(x^2 \pm \frac{8\alpha\beta b_{\mathrm{IR}}}{Z_1^{\mathrm{IR}}} x - \nu_2^2\right) q_\pm(x) = 0 \,, \qquad \beta \neq 1 \tag{4.16}$$

with $\nu_2 = \frac{1+\beta}{2}$. The first equation is again the Bessel equation, and the associated conductivity will be of the form (4.13). The second equation can be also solved analytically, and its infalling solution is

$$q_\pm = e^{ix} x^{\nu_2} U\left(\nu_2 + 1/2 \mp i \frac{4\alpha b_{\mathrm{IR}}}{Z_1^{\mathrm{IR}}} \beta, 2\nu_2 + 1, -2ix\right) \,, \tag{4.17}$$

where U is the hypergeometric confluent function. Using again the method of matching asymptotes we find the scaling for the conductivity for the critical case, which turns out to be

$$\mathrm{Re}\,\sigma_{xx} = \mathrm{Re}\,\sigma_{yy} \propto \omega^\beta \,. \tag{4.18}$$

Even when considering a general action of the type (2.8), the general picture does not change much with respect to the observations of [24]. The anomalous Hall conductivity preserves its form, and it is not vanishing if and only if the time reversal breaking parameter b flows in the IR to a non zero value. In the aforementioned paper the system shows a quantum phase transition when the parameter M/b is suitably tuned, and the anomalous Hall conductivity plays the role of an order parameter.

4.3 Full frequency dependence of conductivities

Now we will turn to the computation of the full frequency dependence of the conductivities. To do so it is necessary to obtain the full $r-$dependence of the background fields, forcing us to select specific functions for Z_1, Z_2, W. We fix them to be $Z_1 = Z_2 = 1$ and $W = q^2\chi^2$, considering that the qualitative behavior of the system is expected to be independent of their form.[7] We will also choose the same scalar potential as in [24]

$$V(\chi) = -12 - 3\chi^2 + \frac{\lambda}{2}\chi^4 \,, \tag{4.19}$$

with $q = \sqrt{3}$, $\lambda = 15/8$.[8] We also fix the flavor number $N = 4$ (eq. (2.4)).[9]

Once all the free functions and the parameters in the action are fixed, the near IR fields reduce to:

---

[7]Defining the functions in this way makes the action (2.8) equivalent to the one used in [24].

[8]We take those values for q and λ to simplify the numerical problem. For such q and λ the IR scaling dimensions for the scalar and axial operators Δ_{IR}'s are integers, simplifying the near IR expansions.

[9]We choose this N because TaAs [1] has precisely eight Weyl points close to the Fermi level, therefore the number of Dirac fermions needed is four.

- Critical point

$$u(r) = u_0 r^2 \left(1 + u_1 r^\alpha + \dots\right) , \qquad h(r) = h_0 r^{2\beta} \left(1 + h_1 r^\alpha + \dots\right) , \qquad (4.20)$$

$$A_z(r) = r^\beta \left(1 + a_1 r^\alpha + \dots\right) , \qquad \chi(r) = \chi_{\text{IR}} \left(1 + \chi_1 r^\alpha + \dots\right) \qquad (4.21)$$

where

$$u_0 \sim 1.193 , \qquad h_0 \sim 1.376 , \qquad \chi_{\text{IR}} \sim 0.661 , \qquad \beta \sim 0.733 \qquad (4.22)$$

$$u_1 \sim 0.177 \chi_1 , \qquad h_1 \sim -1.310 \chi_1 , \qquad a_1 \sim 0.546 \chi_1 , \qquad \alpha = 1.174 .$$

After integrating out to the boundary, the solution has the following ratio for the couplings

$$\bar{M}_c = \frac{M_c}{b_c} \sim 0.868 . \qquad (4.23)$$

From now on we will use the notation $\bar{f}$ to denote the quantity f in units of b.

- Trivial phase

$$u(r) = u_0 r^2 + \dots , \qquad h(r) = h_0 r^2 + \dots , \qquad (4.24)$$

$$A_z(r) = r^{\Delta_{b_{\text{IR}}}} + \dots , \qquad \chi(r) = \chi_{\text{IR}}(1 + \chi_1 r^{-4 + \Delta_{\chi_{\text{IR}}}} + \dots) \qquad (4.25)$$

where

$$u_0 = \frac{6}{5} , \quad \chi_{\text{IR}} = 2\sqrt{\frac{2}{5}} , \quad \Delta_{b_{\text{IR}}} = 2 , \quad \Delta_{\chi_{\text{IR}}} = 5 . \qquad (4.26)$$

The two shooting parameters to build the full solution are (h_0, χ_1), however the underlying conformal invariance of the system implies that the background will be a mono-parametric solution depending on $\bar{M} > \bar{M}_c$.

- Topological phase

$$u(r) = u_0 r^2 + \dots , \qquad h(r) = h_0 r^2 + \dots , \qquad (4.27)$$

$$A_z(r) = 1 + \dots , \qquad \chi(r) = \chi_1 r^{-3/2} e^{-s/r} + \dots \qquad (4.28)$$

where

$$u_0 = 1 , \quad s = \sqrt{\frac{3}{h_0}} . \qquad (4.29)$$

This phase is characterized by having $\bar{M} < \bar{M}_c$. The shooting parameters are h_0, χ_1.

After having constructed the background geometries we can proceed to solve the equations for fluctuations (B.5)–(B.9). To do so, we find a near IR expansion for the gauge field fluctuations and use them to integrate from the IR to the UV. Then, we plug them into (4.8) and extract the conductivities.

The first case to consider is the conductivity in the longitudinal sector, which is shown in figure 1. We computed the conductivity for critical solution (green) and we observe the expected behavior $\omega^{2-\beta}$. In the topological and trivial semimetal phases we observe, as
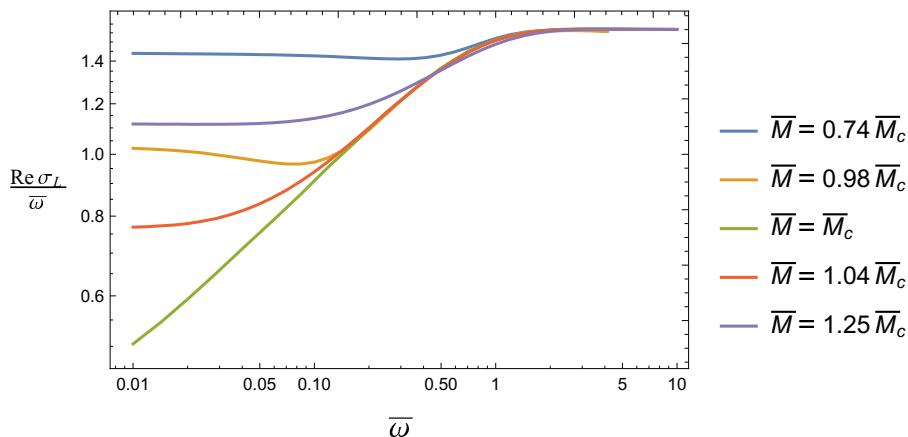
Figure 1. Real part of the longitudinal conductivity as a function of frequency for different values of $\bar{M}$ in the topological and trivial semimetal phases, also the conductivity for the critical point is shown.

expected, a linear frequency dependence at small frequencies.[10] However when $\bar{M}$ is close to the critical value in both phases we observe the emergence of an intermediate scaling given by the critical exponent β.

In figure 2 we show the frequency dependence of the transverse electrical conductivity (left) and the anomalous Hall conductivity (right). We have computed the conductivities for $\bar{M} \sim \bar{M}_c$ in the topological and trivial phases besides the critical $\bar{M}_c$ case. As also observed in figure 1, both phases show a linear conductivity in the IR and UV, and they agree for some intermediate regime with the critical conductivity. The conductivity in the critical phase shows a scaling exponent that agrees very well with the predicted value ω^β. In the right plot, we observe how the anomalous Hall conductivity approaches zero in the critical and trivial phases, unlike the topological phase in which the DC conductivity is non zero. At high frequencies the anomalous Hall conductivity always takes the value $\sigma_{AH}^{(\text{UV})} = 8\alpha b$, this result is not unexpected considering that when the energies are high enough the system should behave as massless, and axial symmetry must be restored (modulo the anomaly breaking term).

Considering the observation of emergence of the critical scaling in the conductivity for $\bar{M} \sim \bar{M}_c$, we computed the conductivity as a function of $(\bar{\omega}, \bar{M})$, in order to sketch the quantum phase diagram of the system using the AC conductivity of the material.[11] In figure 3 we show in a contour plot the quantity

$$m = \omega \frac{d}{d\omega} \log \sigma_L \,, \qquad (4.30)$$

which gives the exponent of the conductivity within the regions where it shows a power-law, otherwise is a meaningless ω-dependent function.[12] Notice that in the regions where m is

---

[10]Notice that the conductivity is divided by $\bar{\omega}$ to make clear the two different scalings, the linear and the critical ones.

[11]In [35] the optical conductivity was also used to reconstruct the quantum phase diagram on a disordered Weyl Semimetal.

[12]We only analyse the longitudinal conductivity, the transverse conductivity should reproduce qualitatively similar results.
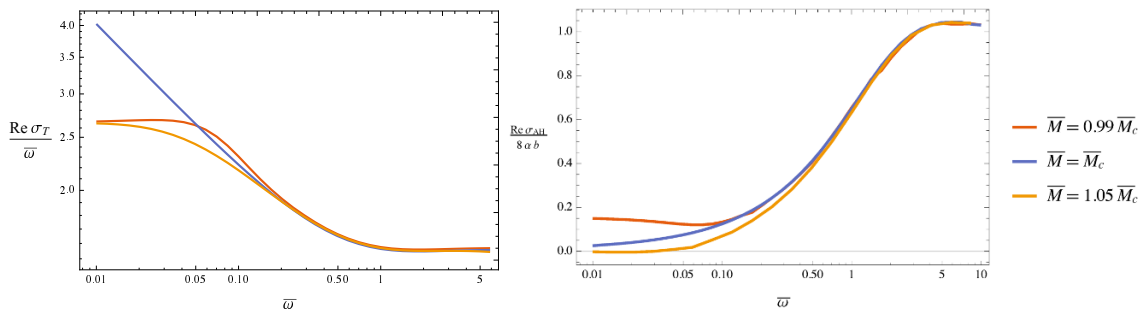
Figure 2. Left: transverse conductivity as a function of frequency for the two different phases of the model and the critical point. Right: anomalous Hall conductivity as a function of the frequency in the topological phase, the quantum critical point and in the trivial phase.

not a constant we observe in the figure a gradient in the colors. In the plot we observe the presence of the quantum critical point and a well defined quantum critical region (red area), extending up to some orders of magnitude above $\omega = 0$. We could expect to reproduce the phase diagram of the system with this computation, due to the underlying scale invariance of the system. At zero temperature the conductivity has to be a function of the form $\sigma(\omega, b, M) = f(\bar{\omega}, \bar{M})$. On the other hand, at zero frequency but finite temperature, the energy scale is given by $\bar{T}$. Therefore for the finite T and $\omega = 0$ case, the power law in frequency observed at $T = 0$ has to be preserved interchanging $\omega \leftrightarrow T$.

The phase diagram shows four well defined regions that can be understood in terms of the physical scales of the problem.

First we have the UV region (upper green) when the energies are large, $\omega \gg b$. The second region corresponding to the Weyl semimetal phase (left green) is manifest at energies smaller than the physical separation of the Weyl cones $\omega \ll b_{\mathrm{IR}}$. In the figure we also included a dashed black line representing the separation of the cones as a function of the mass parameter, and we observe how it determines the transition region between the Weyl semimetal and the quantum critical phases. The trivial semimetal phase (right green region) is characterized by energies much smaller than the UV cut-off. In summary, in order for the quantum critical region to be manifest in the conductivity, the separation of the Weyl nodes has to be much smaller than the UV cut-off scale.

5 Phenomenological implications

A recent experiment [1] measured the optical conductivity of a recently discovered Weyl semimetal (TaAs), in particular when the temperature is $T = 5K$ three differentiated regimes were observed (see right plot of figure 4):

- A Drude peak up to frequencies $\omega \sim 10 \, \mathrm{meV}$

- Between $\omega \sim 10 - 30 \, \mathrm{meV}$ a linear dependence with a slope of $56.7 \, (\Omega \ \mathrm{cm})^{-1}/\mathrm{meV}$

- Between $\omega \sim 30 - 120 \, \mathrm{meV}$ a linear dependence with a slope of $4.1 \, (\Omega \ \mathrm{cm})^{-1}/\mathrm{meV}$.
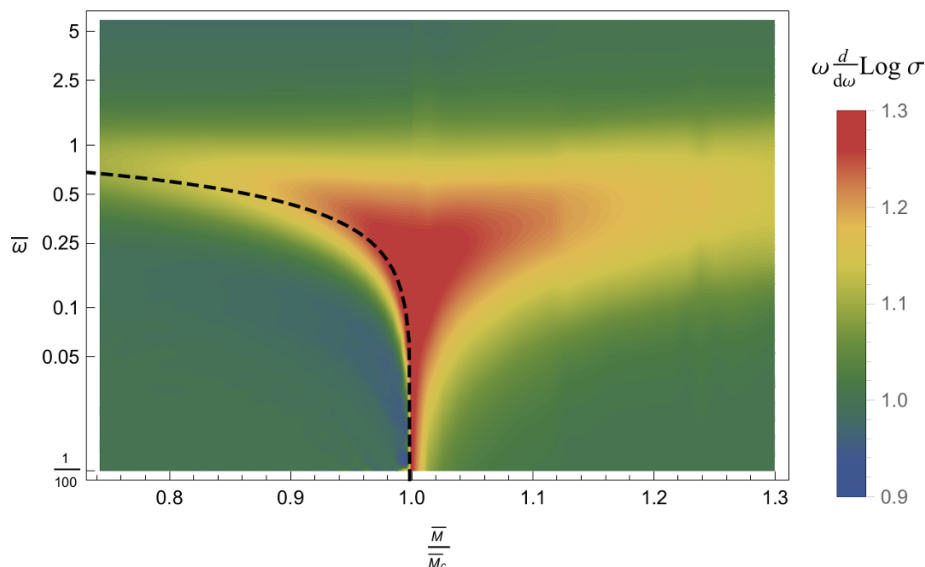
Figure 3. Reconstruction of the quantum phase transition by computing the regions in which the conductivity shows a powerlaw. In the vertical axes we plot the energy scale, given by the frequency, and in the horizontal axes the mass parameter $\bar{M}$. The green regions correspond with a linear conductivity and the red zone to the quantum critical region where the power law is determined by exponent of the quantum critical point β.

Actually, the aspects that concern to us are the two last items. A Drude peak would have been appeared in the holographic model after switching on temperature, introducing chemical potential and breaking translational invariance. Nonetheless our goal is to understand the power-laws of the conductivity and the mechanism that leads to the change in the slope at $\omega \simeq 30\,\mathrm{meV}$. This last aspect is possibly the most interesting one, since the small frequency behavior ($\omega \lesssim 30\,\mathrm{meV}$) is already well described by the predictions of the weak coupling computations [17, 19], while a satisfactory description of the high energy regime is still missing. Considering that $\omega \gg T$ is the region of interest, we can expect to describe the physics with a zero temperature computation. Moreover, the persistence of a linear behavior in the conductivity up to $120\,\mathrm{meV}$ suggests that in this regime the physics of the system is dominated by the low energy linear dispersion relation around the Weyl points. Actually this condition is necessary in order for the IR physics of our holographic description to be applicable to the measurement; we shall further comment on this point below.

Theoretical models in agreement with experiments showed the presence of twelve pairs of Weyl points close to the Fermi energy in the band structure of TaAs [36, 37]. Four pairs, denoted as W1, lie $2\,\mathrm{meV}$ above the Fermi energy. The remaining eight pairs (W2) are $21\,\mathrm{meV}$ below the Fermi energy. For small enough frequencies only the physics close to the W1 points is relevant since the interband transitions near the W2 points require energies of at least $42\,\mathrm{meV}$. A possible explanation of the change in the slope in the linear behavior of the conductivity for $\omega \gtrsim 30\,\mathrm{meV}$ could then be related to the fact that at such energies also the physics near the W2 points starts to contribute. However this interpretation leads
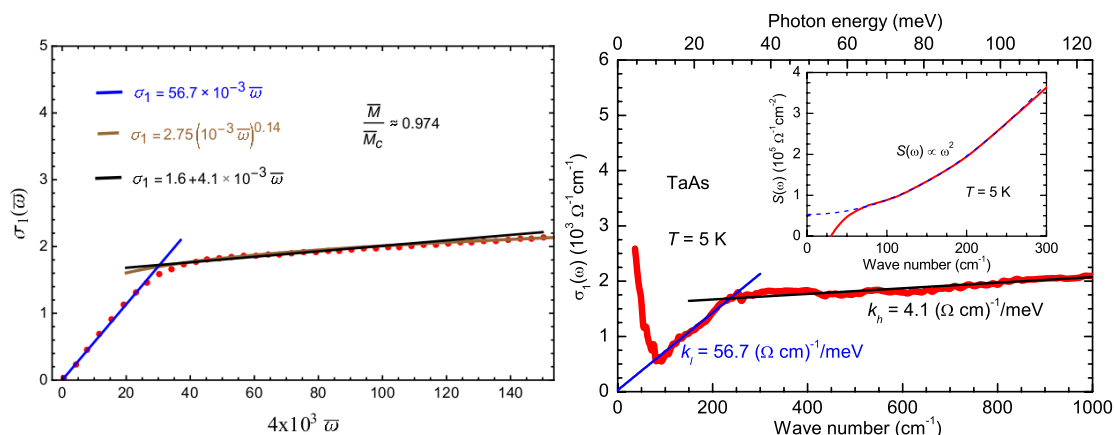
Figure 4. Left plot: transverse conductivity as a function of the conductivity ($\sigma_1 = 10.7 \, \mathrm{Re}\, \sigma_T$). Right plot: experimental data (image taken from [1]), σ_1 is the real part of the conductivity along the (107) surface of the BZ. In the left plot blue and black lines correspond with the fitting used in the right plot. Brown line is the fitting using the dynamical exponent $\beta = 0.14$.

to a tension between the fitting of the Fermi velocity from the data using eq. (1.1) and the reasonable range of values expected for the Fermi velocity derived both theoretically and experimentally.

Motivated by the results of our model, we were tempted to propose a different explanation for the higher frequencies regime of the optical conductivity. We will consider the possibility that it is determined by the quantum critical region of the phase diagram of the material. As observed in figure 3 the scaling in conductivity is different from the linear behavior for energies sitting inside the quantum critical region, i.e. energies higher than the cones separation, but smaller than the UV cut-off. In particular, within our framework the conductivity scaling in the quantum critical region is given by

$$\sigma_L \sim \omega^{2-\beta}, \qquad \sigma_T \sim \omega^{\beta}, \tag{5.1}$$

and β will take always values between $(0, 1)$. If we choose $q = 49/100$ and $\lambda = 1/30$, the critical exponent and mass are

$$\beta \approx 0.14 \quad \implies \sigma_T \sim \omega^{0.14}, \quad \sigma_L \sim \omega^{1.86}, \tag{5.2}$$

$$\bar{M}_c \approx 0.664. \tag{5.3}$$

With this critical exponent it is difficult to distinguish, in the transverse conductivity, between an (almost horizontal) straight line and $\omega^{0.14}$ as we show in figure 4. In the left plot of the aforementioned figure we observe the transverse conductivity for $\bar{M} = 0.647$, noticing a great similarity with the experimental conductivity along the (107) surface of the Brillouin zone (BZ) of the material (right plot). On the other side, the longitudinal conductivity has a complete different behavior as can be seen in figure 5, where the conductivity is almost parabolic. Another important feature is that the longitudinal conductivity is two orders of magnitude smaller than the transverse one, because $\omega^{1.86}$ at small frequencies decays much faster than $\omega^{0.14}$. However, due to the higher amount of Weyl points in the real material
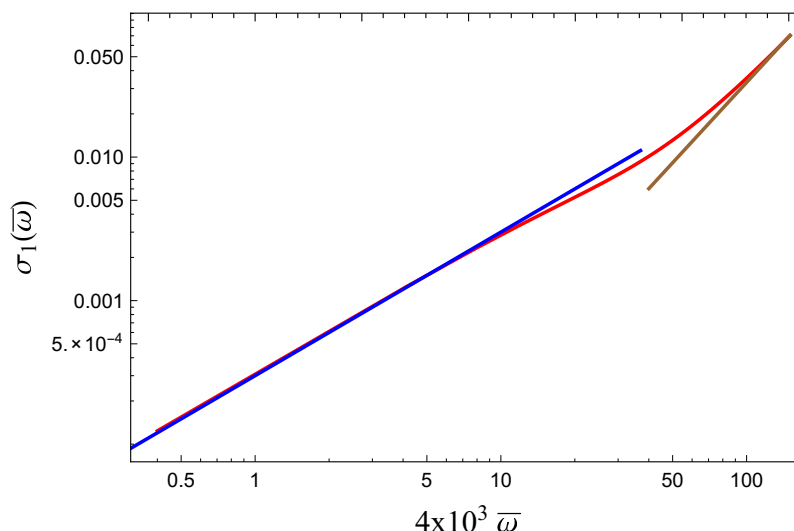
Figure 5. Real part of the longitudinal conductivity (red line) as a function of frequency. Blue line corresponds with a linear fitting and brown line with the critical exponent $\omega^{1.86}$. ($\sigma_1 = 10.7 \, \mathrm{Re} \, \sigma_L$).

and their distribution in momentum space, the same notion of transverse and longitudinal conductivity is absent. In a more realistic holographic setup (more than two unaligned Weyl nodes) the conductivity will not split into transverse and longitudinal, but the effects of the quantum critical point will remain. A more realistic model needs to be studied in detail, in order to check whether the new critical exponent would be compatible with the experimental data.

Although our model has to be simply understood as a toy model for real Weyl semimetals, the results it provides suggest a novel explanation for the high-frequency behavior of the optical conductivity. According to the latter the change in the slope for TaAs at energies $\sim 30 \, \mathrm{meV}$ would not be determined by the physics near the W2 points, but rather by the occurrence of the transition from the Weyl semimetal phase to the critical region. Nevertheless it is worth noticing that in order to trust this interpretation we need to understand the hierarchy of scales in the system. As seen in figure 3 the scale at which the system enters in the critical region is set by the separation of the Weyl points in the momentum space. If this scale happens to be much larger than the energy at which the interband transitions near the W2 nodes turn on ($42 \, \mathrm{meV}$) we obviously cannot rely on this explanation. However, the theoretically predicted values for the separation of Weyl nodes W1 and W2 respectively are [37]

$$b_1 \sim 0.03 \, \text{Å}^{-1} \,, \qquad b_2 \sim 0.07 \, \text{Å}^{-1},$$ (5.4)

which via the dispersion relation $\omega = v_f k$, and after using $v_f^{(1)} \sim 0.3 - 1.7 \, \mathrm{eVÅ}$, $v_f^{(2)} \sim 0.2 - 2.4 \, \mathrm{eVÅ}$ [38, 39] give the energy scales

$$E_{b_1} \sim 8 - 40 \, \mathrm{meV} \,, \qquad E_{b_2} \sim 14 - 160 \, \mathrm{meV} \,,$$ (5.5)

energies which roughly sit within the frequencies studied in the experiment, and comparable also to the energy scale of the interband transitions near the W2. This fact does not rule out the possibility of having a contribution from the quantum critical region of the system on the second slope. Of course this conclusion has to be taken with great care. The holographic model we have used takes only into account the presence of two Weyl cones, whereas the physical system has the set of W1 and W2 nodes with different separations. This fact will imply that conductivities will not be decomposed in term of longitudinal and transverse respect to the cone's separation, and the critical exponents may be modified in a more realistic model. However, the presence of a quantum phase transition will remain, and the effects of the quantum critical region on the optical conductivity shall be present.

Besides the separation of the Weyl points with opposite chirality within W1 or W2, which, as we argued, defines the energy scale associated to the transition to quantum critical region, another relevant scale in the system is given by the separation between pairs of W1 with the ones of W2 (see figure 3 in [37]). This distance roughly determines the UV cut-off of the system where the low energy description (relativistic Weyl fermions) ceases to be valid, since it sets the scale where the deviations from the linearity in the dispersion relation appear.[13] From [38] it turns out that this separation is one order of magnitude bigger than b_2, supporting the explanation for the second slope suggested by the model.

A clear way of testing our proposal would be to tune the analog of $\bar{M}$ in the material and to measure the conductivity. In such an experiment, if the second slope is associated to the quantum critical region, the farther the system is from the quantum critical point the higher the transition scale will be. Unfortunately in TaAs it is not clear how to control experimentally the phase transition [40]. Recently, another material showing a tunable type II Weyl semimetal phase ($Mo_xW_{1-x}Te_2$) has been predicted [40] and experimentally discovered [41]. It would be highly interesting to see what is the behavior of the conductivity in such a type of material.

6 Conclusions

We have generalized the study of [24] analysing the possibility of having Weyl semimetal phases in holography by using the general action

$$S_0 = \int d^5x \sqrt{-g} \left[R - \mathcal{V}(\chi) - \frac{1}{4}Z_1(\chi)H^2 - \frac{1}{4}Z_2(\chi)F^2 - (\partial\chi)^2 + W(\chi)A^2 \right.$$
$$\left. + \frac{\alpha}{3}\epsilon^{MNRPQ}A_M\big(F_{NR}F_{PQ} + 3H_{NR}H_{PQ}\big) \right] , \quad (6.1)$$

within this framework we have proved that Weyl semimetal phases are allowed if the gauge field is massless in the IR, the scalar field runs to a constant value and simultaneously extremizes the scalar potential and gauge field mass function. Another general result is the

---

[13]The reader may wonder why we use this separation and not b_1 and b_2 as an estimate for the cut-off. The reason is that within the model the separation of points with opposite chirality sets the transition in the power-law, even though at this scale there is already a deviation from linearity.

existence of a quantum critical point with a Lifshitz-like scaling symmery and dynamical exponent β, which always takes values between zero and one. We also observed that if the scalar runs to a constant value, the quantum phase transition will be always between the Weyl semimetal phase and a topologically trivial semimetal.

After the classification of the IR fixed points we computed the optical conductivity of the system in all the phases obtaining a linear conductivity in the IR as expected by dimensional analysis, however the presence of the quantum critical point in the phase diagram introduces a quantum critical region in which the conductivity has a scaling given by the dynamical exponent β. The time-reversal breaking parameter breaks the isotropy of the space-time leading in the IR to an anisotropic conductivity given by

$$\sigma_L \sim \omega^{2-\beta}\,, \tag{6.2}$$

$$\sigma_T \sim \omega^{\beta}\,. \tag{6.3}$$

We also verified that the anomalous Hall conductivity obeys an universal form

$$\sigma_{AH} = 8\alpha b_{\mathrm{IR}}\,, \tag{6.4}$$

with b_{IR} being the renormalized time-reversal parameter, which we interpreted as the effective separation of Weyl cones. The universality of the result does not come as a surprise considering that it is intimately related with the anomaly, and it is well known that this type of transport coefficients are protected.

We reconstructed the phase diagram of the theory by computing the power-laws exponents as a function of $\bar{M}$. Remarkably enough the phase diagram showed the standard features of a quantum phase diagram, with a quantum critical region that extends several orders of magnitude above the zero energy case.

Finally we compared our results with the experiment [1]. The experimental data has been qualitatively reproduced within our model after setting the parameters in such a way of having a quantum critical region, characterized by a small critical exponent $\beta = 0.14$. Whether the physics determining the second slope in the right plot of figure 4 is given by the quantum critical region or not can be verified by properly measuring the matrix of conductivities and varying the coupling $\bar{M}$, this tuning would shift the transition scale depending on how far from the critical point the system is.

In the future it would be worth studying a more realistic phase diagram. To do so it would be necessary to consider IR geometries with a logarithmic running for the scalar field, allowing the system to have different IR fixed points, like Lifshitz and hyperscaling violating Lifshitz geometries, which may be insulating. It would be also interesting the inclusion of extra gauge fields in order to model the presence of more than two Weyl nodes.

Acknowledgments

to the Galileo Galilei Institute for theoretical physics, for the hospitality when finishing the present work.

A Gibbons-Hawking action and counterterm

In this appendix we show the explicit form of the Gibbons-Hawking boundary action,

$$S_{GH} = \int_{r=\Lambda} \mathrm{d}^4x \sqrt{-\gamma}\, 2K\,, \tag{A.1}$$

and the counterterm needed to renormalize the theory in the case of having $Z_1 = Z_2 = Z_3 = 1$ and the scalar potential eq. (4.19)

$$S_{CT} = \int_{r=\Lambda} \mathrm{d}^4x \sqrt{-\gamma} \left(\frac{1}{2}\mathcal{V}_{\mathrm{UV}} - |\phi|^2 + \log r \left[\frac{1}{4}F^2 + \frac{1}{4}H^2 + |D_\mu\phi|^2 + \left(\frac{1}{3} + \frac{\lambda}{2}\right)|\phi|^4 \right] \right), \tag{A.2}$$

where $\gamma_{\mu\nu}$ is the induced boudary metric and K the trace of the extrisic curvature.

B Equations of motion

The equations of motion for the action (2.8) can be written as follow

$$R_{MN} + \frac{Z_2}{2}F_{MR}F^R{}_N + \frac{Z_1}{2}H_{MR}H^R{}_N - \partial_M\chi\partial_N\chi + WA_MA_N +$$
$$\frac{g_{MN}}{2}\left[(\partial_M\chi)^2 + \mathcal{V} - R + \frac{Z_2}{4}F^2 + \frac{Z_1}{4}H^2 - WA^2\right] = 0\,, \tag{B.1}$$

$$\frac{1}{\sqrt{-g}}\partial_M\left(\sqrt{-g}\,Z_1H^{NM}\right) - 2\alpha\,\epsilon^{NMRPQ}F_{MR}H_{PQ} = 0\,, \tag{B.2}$$

$$\frac{1}{\sqrt{-g}}\partial_M\left(\sqrt{-g}Z_2F^{NM}\right) - \alpha\epsilon^{NMRPQ}\left[F_{MR}F_{PQ} + H_{MR}H_{PQ}\right] - 2WA^N = 0\,, \tag{B.3}$$

$$\frac{1}{\sqrt{-g}}\partial_M\left(\sqrt{-g}\,\partial^M\chi\right) = \frac{1}{8}\partial_\chi Z_1H^2 + \frac{1}{8}\partial_\chi Z_2F^2 + \frac{1}{2}\partial_\chi WA^2 + \frac{1}{2}\partial_\chi\mathcal{V}\,. \tag{B.4}$$

After plugging the ansatz (3.1) into the previous equations we obtain for the gravity sector

$$\frac{Z_2A_3'^2}{2h(r)} + \frac{h''}{2h} - \frac{h'^2}{4h^2} + \frac{u''}{u} - \frac{u'^2}{2u^2} + \chi'^2 = 0\,, \tag{B.5}$$

$$-\frac{Z_2A_3'^2}{4h} + \frac{A_3^2W}{2hu} + \frac{3u'}{4u}\left(\frac{h'}{h} + \frac{u'}{u}\right) + \frac{\mathcal{V}}{2u} - \frac{1}{2}\chi'^2 = 0\,, \tag{B.6}$$

$$\frac{Z_2A_3'^2}{2h} + \frac{WA_3^2}{hu} + \frac{u'}{2u}\left(\frac{3h'}{2h} - \frac{u'}{u}\right) - \frac{h'^2}{4h^2} + \frac{h''}{2h} - \frac{u''}{2u} = 0\,, \tag{B.7}$$

only two of them are linearly independent. The gauge sector reads

$$\sqrt{h}\left(\frac{u^2Z_2A_3'}{\sqrt{h}}\right)' - 2uWA_z = 0\,, \tag{B.8}$$

and the scalar

$$\frac{1}{\sqrt{h}u}\left(\sqrt{h}u^2\chi'\right)' - \partial_\chi Z_2\frac{uA_3'^2}{4h} - \partial_\chi W\frac{A_3^2}{2h} - \frac{1}{2}\partial_\chi\mathcal{V} = 0\,. \tag{B.9}$$

C IR perturbations

Assuming the following ansatz for the fields

$$ds^2 = u(r)(-dt^2 + dx_1^2 + dx_2^2) + h(r)dx_3^2 + \frac{dr^2}{u(r)}, \qquad (C.1)$$

$$A = A_3(r)dx_3, \qquad (C.2)$$

$$\chi = \chi(r), \qquad (C.3)$$

the solutions can be split into a leading and subleading contribution in the IR

$$u(r) = u_0 r^2 \left(1 + \delta u(r) + \ldots\right), \qquad h(r) = h_0 r^{2\beta} \left(1 + \delta h(r) + \ldots\right), \qquad (C.4)$$

$$A_3(r) = r^c(b_{\mathrm{IR}} + \delta A_r(r) + \ldots), \qquad \chi(r) = \chi_{\mathrm{IR}} + \delta\chi(r) + \ldots \; . \qquad (C.5)$$

The solutions for the subleading IR corrections can be obtained for each phase of the model.

- *Weyl Semimetal Phase* ($b_{\mathrm{IR}} = 1$, $c = 0$): corrections to the Weyl semimetal phase are of the following type

$$\delta u = \frac{c_1}{r} + \frac{c_2}{r^4}, \qquad \delta h = \frac{c_1}{r} - \frac{2c_2}{r^4} + c_3, \qquad \delta A_3 = c_4 + \frac{c_5}{r^2}, \qquad (C.6)$$

c_3, c_4 are marginal deformations that just redefine the value of h_0 and b_{IR} respectively and can be scaled out. The rest of the modes are relevant and will destroy the AdS IR geometry.

The only perturbation with an irrelevant deformation is the scalar field

$$\delta\chi = c_6 r^{-3/2} e^{-\frac{s}{r}} + c_7 r^{-3/2} e^{\frac{s}{r}}, \qquad (C.7)$$

where $s = \sqrt{1/2 W_{\mathrm{IR}}'' h_0^{-1}} L_{\mathrm{IR}}$. If $W_{\mathrm{IR}}'' < 0$ any perturbation would destroy the IR. On the other hand if $W_{\mathrm{IR}}'' > 0$ the perturbation associated to c_6 would be irrelevant in the IR.

- *Trivial Semimetal Phase* ($b_{\mathrm{IR}} = 0$, $c = 0$): corrections to the trivial semimetal phase are of the following type

$$\delta u = \frac{c_1}{r} + \frac{c_2}{r^4}, \qquad \delta h = \frac{c_1}{r} - \frac{2c_2}{r^4} + c_3. \qquad (C.8)$$

These perturbations have the same form as in the previous case, and have to be all set to zero. However the scalar and gauge field have irrelevant modes

$$\delta A_3 = c_4 r^{-2-\Delta_{b_{\mathrm{IR}}}} + c_5 r^{\Delta_{b_{\mathrm{IR}}}}, \qquad (C.9)$$

where $\Delta_{b_{\mathrm{IR}}} = -1 + \sqrt{1 + \frac{2 W_{\mathrm{IR}} L_{\mathrm{IR}}^2}{Z_2^{\mathrm{IR}}}}$. c_4 corresponds to a relevant deformation, but c_5 is irrelevant. With the scalar field something similar happens; one mode is relevant and the other one irrelevant

$$\delta\chi = c_6 r^{-\Delta_{\chi_{\mathrm{IR}}}} + c_7 r^{-4+\Delta_{\chi_{\mathrm{IR}}}}, \qquad (C.10)$$

where $\Delta_{\chi_{\mathrm{IR}}} = 2 + \sqrt{4 + m_{\mathrm{IR}}^2 L_{\mathrm{IR}}^2}$. Stability implies $m_{\mathrm{IR}}^2 L_{\mathrm{IR}}^2 > 0$. We are using here the definition $\mathcal{V}_{\mathrm{IR}}'' = 2 m_{\mathrm{IR}}^2$.

- *Critical Point* ($b_{\text{IR}} = 1$, $c = \beta$): in the critical case, the zero temperature deformation to the Lifshitz IR takes the following form

$$\delta u = u_1 r^\alpha, \qquad \delta h = h_1 r^\alpha, \qquad \delta A_3 = a_1 r^\alpha, \qquad \delta\chi = \chi_{\text{IR}}\chi_1 r^\alpha, \qquad \text{(C.11)}$$

where χ_1 is the only free constant. The rest is

$$u_1 = \frac{2(\beta-1)\chi_{\text{IR}}\left(3\beta^2 u_0 Z'_{\text{IR}} - 2(\alpha+2\beta-1)W'_{\text{IR}}\right)}{3(\alpha+1)\beta u_0\left(\alpha^2 + \alpha(\beta+3) - 2(\beta-3)(\beta-1)\right)Z_{\text{IR}}}\chi_1 \qquad \text{(C.12)}$$

$$h_1 = \frac{8\chi_{\text{IR}}(\beta-1)\left(\alpha^2 + 3\alpha\beta + \alpha + \beta(\beta+2)\right)W'_{\text{IR}}}{3\alpha(\alpha+1)\beta u_0\left(\alpha^2 + \alpha(\beta+3) - 2(\beta-3)(\beta-1)\right)Z_{\text{IR}}}\chi_1 +$$
$$-\frac{6\chi_{\text{IR}}\beta^2 u_0(\beta-1)(\alpha(\alpha-\beta+7)+6)Z'_{\text{IR}}}{3\alpha(\alpha+1)\beta u_0\left(\alpha^2 + \alpha(\beta+3) - 2(\beta-3)(\beta-1)\right)Z_{\text{IR}}}\chi_1 \qquad \text{(C.13)}$$

$$a_1 = \frac{2\chi_{\text{IR}}\left(3\alpha^2 + \alpha(6\beta-3) + 2\left(\beta^2+\beta-2\right)\right)W'_{\text{IR}}}{3\alpha(\alpha+1)u_0\left(\alpha^2 + \alpha(\beta+3) - 2(\beta-3)(\beta-1)\right)Z(\chi_{\text{IR}})}\chi_1 +$$
$$-\frac{\beta\chi_{\text{IR}}(\alpha(\alpha(\alpha+4)-(\beta-7)\beta-3)+6(\beta-1))Z'_{\text{IR}}}{\alpha(\alpha+1)\left(\alpha^2 + \alpha(\beta+3) - 2(\beta-3)(\beta-1)\right)Z_{\text{IR}}}\chi_1. \qquad \text{(C.14)}$$

The exponent α can be obtained inverting the following equation

$$\mathcal{V}''_{\text{IR}} = 2\alpha u_0(\alpha+\beta+3) + \frac{(\beta-1)\beta u_0 Z''_{\text{IR}}}{Z_{\text{IR}}} + \frac{2(\beta-1)W''_{\text{IR}}}{\beta Z(\chi_{\text{IR}})} +$$
$$\frac{4(\beta-1)(\beta+2)W'^2_{\text{IR}}}{3\beta^2 u_0\left(\alpha^2 + \alpha(\beta+3) - 2(\beta-3)(\beta-1)\right)Z^2_{\text{IR}}} +$$
$$\frac{4(\beta-1)(3\beta-5)W'_{\text{IR}}Z'_{\text{IR}}}{\left(\alpha^2 + \alpha(\beta+3) - 2(\beta-3)(\beta-1)\right)Z^2_{\text{IR}}} +$$
$$-\frac{2(\beta-1)\beta u_0\left(\alpha^2 + \alpha(\beta+3) + \beta(11-2\beta) - 6\right)Z'^2_{\text{IR}}}{\left(\alpha^2 + \alpha(\beta+3) - 2(\beta-3)(\beta-1)\right)Z^2_{\text{IR}}}. \qquad \text{(C.15)}$$

The previous polynomial has four possible solutions for α and only two of them may be real numbers, depending on the values of the other parameters.

References

[1] B. Xu et al., *Optical spectroscopy of the Weyl semimetal TaAs*, *Phys. Rev.* **B 93** (2016) 121110 [arXiv:1510.00470].

[2] S.-Y. Xu et al., *Discovery of a Weyl fermion semimetal and topological Fermi arcs*, *Science* **349** (2015) 613 [arXiv:1502.03807].

[3] H.B. Nielsen and M. Ninomiya, *Adler-Bell-Jackiw anomaly and Weyl fermions in crystal*, *Phys. Lett.* **B 130** (1983) 389 [INSPIRE].

[4] D. Kharzeev, *Parity violation in hot QCD: Why it can happen and how to look for it*, *Phys. Lett.* **B 633** (2006) 260 [hep-ph/0406125] [INSPIRE].

[5] D. Kharzeev and A. Zhitnitsky, *Charge separation induced by P-odd bubbles in QCD matter*, *Nucl. Phys.* **A 797** (2007) 67 [arXiv:0706.1026] [INSPIRE].

[6] A. Gynther, K. Landsteiner, F. Pena-Benitez and A. Rebhan, *Holographic Anomalous Conductivities and the Chiral Magnetic Effect*, *JHEP* **02** (2011) 110 [arXiv:1005.2587] [INSPIRE].

[7] V. Fomin, L. Frappat and É. Ragoucy, *Bethe equations for generalized Hubbard models*, *JHEP* **09** (2009) 055 [arXiv:0906.4512] [INSPIRE].

[8] N. Banerjee, J. Bhattacharya, S. Bhattacharyya, S. Dutta, R. Loganayagam and P. Surówka, *Hydrodynamics from charged black branes*, *JHEP* **01** (2011) 094 [arXiv:0809.2596] [INSPIRE].

[9] K. Landsteiner, E. Megias and F. Pena-Benitez, *Gravitational Anomaly and Transport*, *Phys. Rev. Lett.* **107** (2011) 021601 [arXiv:1103.5006] [INSPIRE].

[10] K. Landsteiner, E. Megias, L. Melgar and F. Pena-Benitez, *Holographic Gravitational Anomaly and Chiral Vortical Effect*, *JHEP* **09** (2011) 121 [arXiv:1107.0368] [INSPIRE].

[11] K. Landsteiner, Y. Liu and Y.-W. Sun, *Odd viscosity in the quantum critical region of a holographic Weyl semimetal*, *Phys. Rev. Lett.* **117** (2016) 081604 [arXiv:1604.01346] [INSPIRE].

[12] K. Landsteiner, Y. Liu and Y.-W. Sun, *Negative magnetoresistivity in chiral fluids and holography*, *JHEP* **03** (2015) 127 [arXiv:1410.6399] [INSPIRE].

[13] A. Lucas, R.A. Davison and S. Sachdev, *Hydrodynamic theory of thermoelectric transport and negative magnetoresistance in Weyl semimetals*, *Proc. Nat. Acad. Sci.* **113** (2016) 9463 [arXiv:1604.08598] [INSPIRE].

[14] Q. Li et al., *Observation of the chiral magnetic effect in ZrTe5*, *Nature Phys.* **12** (2016) 550 [arXiv:1412.6543] [INSPIRE].

[15] R. Batabyal et al., *Visualizing weakly bound surface Fermi arcs and their correspondence to bulk Weyl fermions*, *Sci. Adv.* **2** (2016) e1600709.

[16] J. González, *Strong-coupling phases of 3D Dirac and Weyl semimetals. A renormalization group approach*, *JHEP* **10** (2015) 190 [arXiv:1509.00210] [INSPIRE].

[17] A.A. Burkov and L. Balents, *Weyl Semimetal in a Topological Insulator Multilayer*, *Phys. Rev. Lett.* **107** (2011) 127205 [arXiv:1105.5138] [INSPIRE].

[18] B. Roy, R.-J. Slager and V. Juricic, *Global phase diagram of a dirty Weyl semimetal*, arXiv:1610.08973 [INSPIRE].

[19] P. Hosur, S.A. Parameswaran and A. Vishwanath, *Charge Transport in Weyl Semimetals*, *Phys. Rev. Lett.* **108** (2012) 046602 [arXiv:1109.6330] [INSPIRE].

[20] P. Hosur and X. Qi, *Recent developments in transport phenomena in Weyl semimetals*, *Comptes Rendus Physique* **14** (2013) 857 [arXiv:1309.4464] [INSPIRE].

[21] U. Gürsoy, V. Jacobs, E. Plauschinn, H. Stoof and S. Vandoren, *Holographic models for undoped Weyl semimetals*, *JHEP* **04** (2013) 127 [arXiv:1209.2593] [INSPIRE].

[22] V.P.J. Jacobs, P. Betzios, U. Gürsoy and H.T.C. Stoof, *Electromagnetic response of interacting Weyl semimetals*, *Phys. Rev.* **B 93** (2016) 195104 [arXiv:1512.04883] [INSPIRE].

[23] K. Landsteiner and Y. Liu, *The holographic Weyl semi-metal*, *Phys. Lett.* **B 753** (2016) 453 [arXiv:1505.04772] [INSPIRE].

[24] K. Landsteiner, Y. Liu and Y.-W. Sun, *Quantum phase transition between a topological and a trivial semimetal from holography*, *Phys. Rev. Lett.* **116** (2016) 081602 [arXiv:1511.05505] [INSPIRE].

[25] C. Copetti, J. Fernández-Pendás and K. Landsteiner, *Axial Hall effect and universality of holographic Weyl semi-metals*, *JHEP* **02** (2017) 138 [arXiv:1611.08125] [INSPIRE].

[26] V.P.J. Jacobs, S.J.G. Vandoren and H.T.C. Stoof, *Holographic interaction effects on transport in Dirac semimetals*, *Phys. Rev.* **B 90** (2014) 045108 [arXiv:1403.3608] [INSPIRE].

[27] E. Witten, *Anti-de Sitter space and holography*, *Adv. Theor. Math. Phys.* **2** (1998) 253 [hep-th/9802150] [INSPIRE].

[28] C. Charmousis, B. Gouteraux, B. Soo Kim, E. Kiritsis and R. Meyer, *Effective holographic theories for low-temperature condensed matter systems*, *JHEP* **11** (2010) 151 [arXiv:1005.4690] [INSPIRE].

[29] S.S. Gubser and F.D. Rocha, *The gravity dual to a quantum critical point with spontaneous symmetry breaking*, *Phys. Rev. Lett.* **102** (2009) 061601 [arXiv:0807.1737] [INSPIRE].

[30] J. Bhattacharya, S. Cremonini and B. Gouteraux, *Intermediate scalings in holographic RG flows and conductivities*, *JHEP* **02** (2015) 035 [arXiv:1409.4797] [INSPIRE].

[31] B. Goutéraux and E. Kiritsis, *Quantum critical lines in holographic phases with (un)broken symmetry*, *JHEP* **04** (2013) 053 [arXiv:1212.2625] [INSPIRE].

[32] J. Gath, J. Hartong, R. Monteiro and N.A. Obers, *Holographic Models for Theories with Hyperscaling Violation*, *JHEP* **04** (2013) 159 [arXiv:1212.3263] [INSPIRE].

[33] G.T. Horowitz and M.M. Roberts, *Zero temperature limit of holographic superconductors*, *JHEP* **11** (2009) 015 [arXiv:0908.3677] [INSPIRE].

[34] S.S. Gubser and F.D. Rocha, *The gravity dual to a quantum critical point with spontaneous symmetry breaking*, *Phys. Rev. Lett.* **102** (2009) 061601 [arXiv:0807.1737] [INSPIRE].

[35] B. Roy, V. Juricic and S. Das Sarma, *Universal optical conductivity of a disordered Weyl semimetal*, *Nature Sci. Rep.* **6** (2016) 32446 [arXiv:1603.00017].

[36] H. Weng, C. Fang, Z. Fang, B.A. Bernevig and X. Dai, *Weyl semimetal phase in noncentrosymmetric transition-metal monophosphides*, *Phys. Rev.* **X 5** (2015) 011029.

[37] S.-M. Huang et al., *A Weyl Fermion semimetal with surface Fermi arcs in the transition metal monopnictide TaAs class*, *Nature Commun.* **6** (2015) 7373.

[38] X. Huang et al., *Observation of the Chiral-Anomaly-Induced Negative Magnetoresistance in 3D Weyl Semimetal TaAs*, *Phys. Rev.* **X 5** (2015) 031023 [arXiv:1503.01304].

[39] B.Q. Lv et al., *Observation of Weyl nodes in TaAs*, *Nature Phys.* **11** (2015) 724 [arXiv:1503.09188].

[40] T.R. Chang, S.Y. Xu, G. Chang, C.C. Lee and S.M. Huang, *Prediction of an arc-tunable Weyl Fermion metallic state in* $Mo_xW_{1-x}Te_2$, *Nature* **7** (2016) 10639.

[41] I. Belopolski et al., *Discovery of a new type of topological Weyl fermion semimetal state in* $Mo_xW_{1-x}Te_2$, *Nature Commun.* **7** (2016) 1.